Journal of Medicinal Chemistry

pubs.acs.org/jmc

Drug Annotation

Discovery of CMX990: A Potent SARS-CoV-2 3CL Protease Inhibitor Bearing a Novel Warhead

N. G. R. Dayan Elshan,* Karen C. Wolff, Laura Riva, Ashley K. Woods, Gennadii Grabovyi, Katy Wilson, James Pedroarena, Sourav Ghorai, Armen Nazarian, Frank Weiss, Yuyin Liu, Wrickban Mazumdar, Lirui Song, Neechi Okwor, Jacqueline Malvin, Malina A. Bakowski, Nathan Beutler, Melanie G. Kirkpatrick, Amal Gebara-Lamb, Edward Huang, Vân T. B. Nguyen-Tran, Victor Chi, Shuangwei Li, Thomas F. Rogers, Case W. McNamara, Anil Kumar Gupta, Alireza Rahimi, Jian Jeffrey Chen, Sean B. Joseph, Peter G. Schultz, and Arnab K. Chatterjee*

Cite This: *J. Med. Chem.* 2024, 67, 2369−2378

Read Online

ACCESS | Metrics & More | Article Recommendations | Supporting Information

ABSTRACT: There remains a need to develop novel SARS-CoV-2 therapeutic options that improve upon existing therapies by an increased robustness of response, fewer safety liabilities, and global-ready accessibility. Functionally critical viral main protease (M^{pro}, $3CL^{pro}$) of SARS-CoV-2 is an attractive target due to its homology within the coronaviral family, and lack thereof toward human proteases. In this disclosure, we outline the advent of a novel SARS-CoV-2 $3CL^{pro}$ inhibitor, **CMX990**, bearing an unprecedented trifluoromethoxymethyl ketone warhead. Compared with the marketed drug nirmatrelvir (combination with ritonavir = Paxlovid), **CMX990** has distinctly differentiated potency (~5× more potent in primary cells) and human *in vitro* clearance (>4× better microsomal clearance and >10× better hepatocyte clearance), with good *in vitro*-to-*in vivo* correlation. Based on its compelling preclinical profile and projected once or twice a day dosing supporting unboosted oral therapy in humans, **CMX990** advanced to a Phase 1 clinical trial as an oral drug candidate for SARS-CoV-2.

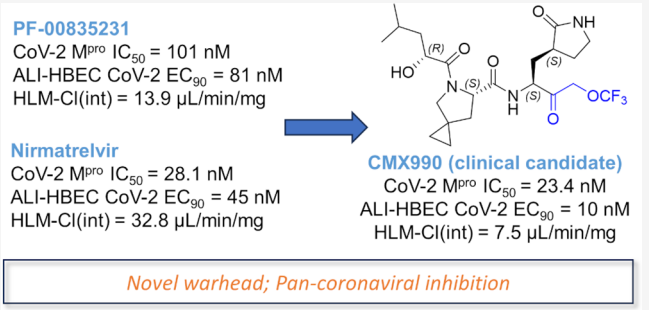

INTRODUCTION

With ~770 million confirmed cases and ~7 million deaths worldwide to date, the SARS-CoV-2 pandemic has had a resounding impact around the globe.[1] While the advent of prophylactic vaccines has helped overcome pandemic status,[2] many health hurdles still remain for those who contract the disease and/or are not vaccinated due to personal, socio-economic, geographic, or other adverse circumstances. On account of this, and to prepare for future pandemics, many drug discovery programs were pursued around the world for post-infection treatment options. Some of the more successful outcomes from such efforts include the drugs remdesivir (Veklury, Gilead Sciences), nirmatrelvir (+ ritonavir = Paxlovid, Pfizer Inc.), ensitrelvir (Xocova, Shionogi & Co.), molnupiravir (Lagevrio, Merck & Co.), and simnotrelvir (+ ritonavir = Xiannuoxin, Simcere Pharmaceutical).[3−7] Although having shown some level of efficacy in clinical trials, each of these therapies has limitations in areas such as robustness of response, therapeutic index, and toxicology, drug−drug interaction (DDI) concerns, affordability, and widespread availability. Therefore, there remains major interest and need to develop alternative therapies for coronaviral infections. Herein, we describe a program that led to the development of a unique SARS-CoV-2 drug candidate that reached a Phase 1 clinical trial.

At the onset of the coronavirus pandemic in 2020, Calibr leveraged its drug repurposing library ReFRAME (Repurposing, Focused Rescue, and Accelerated Medchem),[8] both internally and with external collaborators, to find potential hits that could be quickly adapted as effective antivirals to combat SARS-CoV-2. Via these screens, multiple clinical-stage cysteine/serine protease inhibitors, such as emricasan, VBY-825, and dutacatib (Figure 1A), were found to have moderate SARS-CoV-2 antiviral potency. This made sense as viral $3CL^{pro}$ is a main enzyme involved in SARS-CoV-2 replication, and there is significant homology across various proteases.[9] SARS-CoV-2, belonging to the genus *Betacoronavirus*, encodes four

Received: October 17, 2023
Revised: November 26, 2023
Accepted: January 12, 2024
Published: February 9, 2024

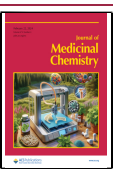

https://doi.org/10.1021/acs.jmedchem.3c01938
J. Med. Chem. 2024, 67, 2369−2378

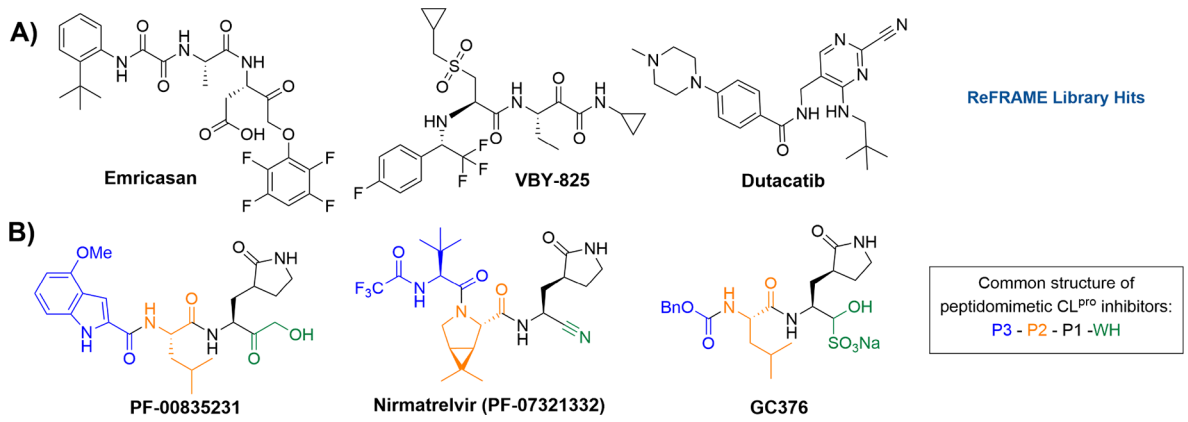

Figure 1. Representative known protease inhibitors. A) Initial ReFRAME library hits identified as moderate (low μM) potency inhibitors of SARS-CoV-2. B) Peptidomimetic SARS-CoV-2 CL^{pro} inhibitors PF-00835231 (Pfizer), PF-07321332 (Pfizer), and GC376 (Anivive). Generally, up to four distinct structural regions are found in all peptidomimetic CL^{pro} inhibitors: warhead (WH), P1 (amino acid 1, recognition element with a lactam side chain), P2 (AA 2), and P3 (a *N*-Cap, or a third AA). Common warheads include hydroxymethyl ketones (e.g., PF-00835231), nitriles (e.g., nirmatrelvir), aldehydes, or bisulfite adducts thereof (e.g., GC376), and aryloxymethyl ketones (e.g., emricasan).

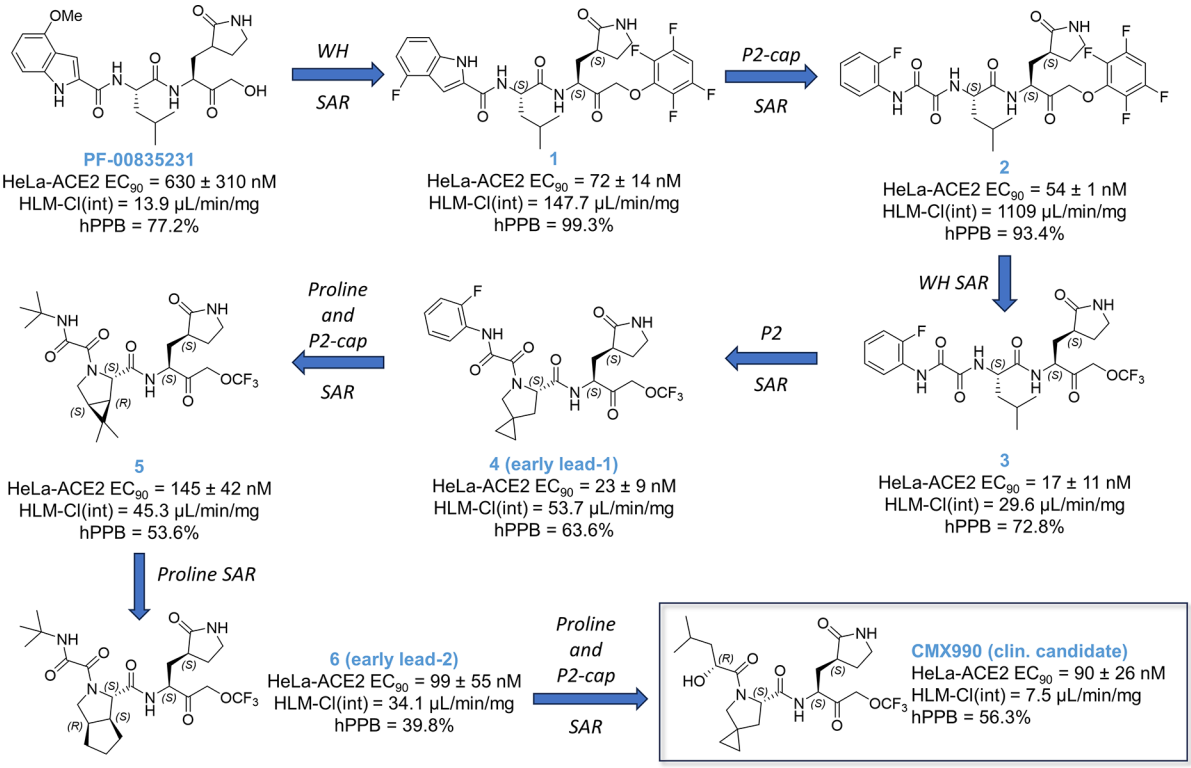

Figure 2. Representative SAR summary trajectory to early program leads, including clinical candidate CMX990. SAR studies across all regions of the compounds were carried out in parallel, leading to a series of >1600 total compounds to date. WH = warhead.

structural proteins (spike, envelope, membrane, and nucleocapsid) and several accessory proteins. The polyproteins pp1a and pp1ab must be cleaved into their individual, non-structural proteins for successful viral replication.[10] Two viral proteases are essential and responsible for processing these polyproteins: the 3C-like protease (3CL protease, 3CL^{pro}, CL^{pro}; also referred to as "main protease", M^{pro}) and a papain-like protease (PL^{pro}).[11]

CL^{pro} cleaves polypeptides after a glutamine residue in the P1 position of the substrate, which is a unique activity not observed in other human proteases and suggests that this viral protease can be specifically and selectively inhibited by a small-molecule inhibitor.[12] The homology between coronaviral main proteases provides an attractive avenue to develop therapeutics that could also be capable of tackling future threats from mutated viral variants, as well as other genera of coronaviruses. CL^{pro} has four active sites (S1′, S1, S2, and S4), which can be accommodated by distinct structural regions of a peptidomimetic substrate/inhibitor amenable for structure−activity relationship (SAR) optimization (Figure 1B): A warhead (WH), P1 (amino acid [AA] 1, recognition element with a lactam side chain), P2 (AA 2), and P3 (a *N*-Cap, or a third AA). The warhead that engages the catalytic site Cys145 plays an important role in the potency of such inhibitors, given that Cys145 is an essential residue for antiviral activity.[13] In addition, it is well established that a glutamine derivative (γ-

https://doi.org/10.1021/acs.jmedchem.3c01938
J. Med. Chem. 2024, 67, 2369−2378

Table 1. Representative Compounds and Profiling Data for CMX990 Series SAR[a]

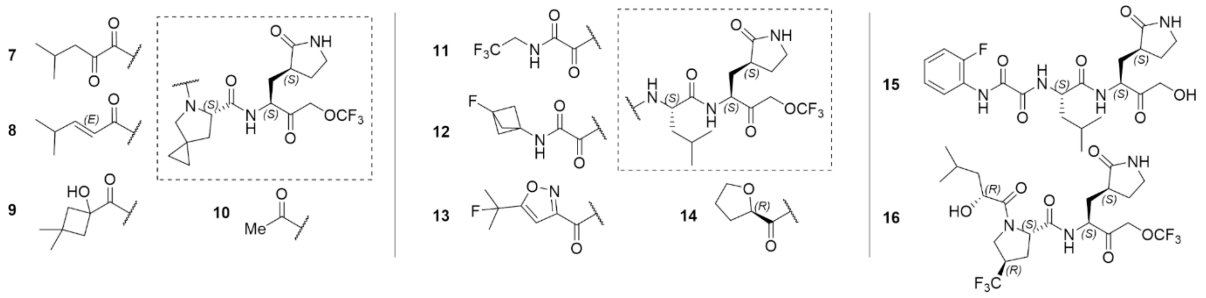

Compound	logD	CoV-2 M^{pro} IC_{50} (nM)	CoV-2 EC_{90} (nM)		hPPB (%)	HLM Cl_{int} (μL/min/mg)	IV PK Cl_p (mL/min/kg)		F(PO) (%)	
			ALI-HBEC	HeLa-ACE2			Mu	Dog	Mu	Dog
1	4.4	n.d.	n.d.	72	99.3	147.7	31.8[a]	–	<1[a]	–
2	3.3	14.8	n.d.	54	93.4	1109.4	47.6[a,b]	50.3	1.3[a,b]	1.5
3	2.8	76.3	133	17	72.8	29.6	173[a]	53.4	<1[a]	21.5
4	2.4	16.1	14.3	23	63.6	53.7	129	28.7	6.3	38.0
5	1.6	81.1	125	145	53.6	45.3	65.9	36.9	32.4	23.4
6	2.0	28.8	19.3	99	39.8	34.2	45.1	38.8	25.2	21.6
7	2.6	24.0	n.d.	117	54.8	62.2	–	36.2	–	–
8	3.0	34.7	n.d.	61	43.5	26.2	53.2[c]	–	51.3[c]	–
9	2.0	36.5	n.d.	108	58.8	16.3	–	40.3	–	–
10	1.3	35.4	n.d.	346	<1	12.8	71.0	11.7	7.2	28.0
11	2.0	34.5	50.8	62	31.7	8.4	35.6[c]	51.8	35.3[c]	35.7
12	1.0	33.7	20.5	24	47.3	17.4	11.1[c]	56.9	20.7[c]	25.0
13	3.6	34.8	14	38	67.5	19.2	n.c.	15.0	2.4	35.3
14	2.0	60.1	51.8	138	34.3	12.2	107	18.4	19.0	48.7
15	0.3	160	n.d.	245	51.8	13.0	n.c.[a]	23.3	4.6[a]	37.7
16	2.6	22.0	n.d.	50	50.1	14.9	19.3[c]	23.7	10.2[c]	57.2
CMX990	**2.3**	**23.4**	**9.6**	**90**	**56.3**	**7.5**	**125**	**23.0**	**14.5**	**52.8**
Nirmatrelvir	1.5	28.1	44.8	148	54.8	21.8	35.8	1.92	53.5	68.7
PF-00835231	1.2	101	81.4	630	77.2	13.9	86.4	–	1.0	–

[a]EC_{90} = 90% effective concentration, Cl_{int} = intrinsic clearance, Cl_p = plasma clearance, F = bioavailability, HLM = human liver microsomes, hPPB = human plasma protein binding, IV = intravenous, Mu = mouse, n.d. = not determined, n.c. = not calculated, PO = per os (oral). Mu data: a = hamster, b = data from close analog, c = rat.

lactam) is highly preferred to occupy the S1 site of cysteine proteases, which not only mimics the P1 glutamine of the native substrates but also increases the activity of inhibitors.[14] Many of these engagement characteristics of coronaviral CL^{pro} were well established in the seminal work done by Pfizer, Inc. and others during the SARS-CoV-1 outbreak, leading to CL^{pro} inhibitor drug candidates such as PF-00835231,[15] which is the active form of one of the very first candidates that went into Phase 1 clinical trials for SARS-CoV-2 treatment.

RESULTS AND DISCUSSION

Extending our ReFRAME starting points via incorporation of literature knowledge of protease inhibitor designs (including caspase/cathepsin literature), we have explored SAR across all regions of this peptidomimetic target template, leading to a library of over 1600 compounds to date.[16] Only a key SAR trajectory (Figure 2) and the performance characteristics of selected representative compounds (Table 1) leading to clinical candidate **CMX990** are highlighted in this disclosure. The SAR evaluations happened across both P2-non-prolines as well as P2-proline derivatives. Key optimization parameters during early development were to improve the potency and human microsomal clearance of PF-00835231. The warhead change from the hydroxymethyl ketone in PF-00835231 to an aryloxymethyl ketone (**1**) led to a ∼9-fold increase in potency (Figure 2). However, the microsomal clearance of this warhead was rapid, leading to low pharmacokinetic (PK) profiles. Opening of the indole ring to get the aryl oxamide analog led to a modest increase in potency, but this made the microsomal clearance worse. A number of additional warheads were screened, including, but not limited to, nitriles, ketoamides, aldehydes, and prodrugs of hydroxymethyl ketone. All these warheads lacked either the potency and/or the clearance (*in vitro*/*in vivo*) profile we were looking for. We therefore decided to develop a novel covalent warhead for this compound series, resulting in trifluoromethoxymethyl ketone warhead compound **3**. Compared to the preceding aryloxymethyl ketone analog **2**, the new warhead analog **3**, resulted in >3× improved potency (HeLa-ACE2 CoV2 EC_{90} = 17 nM) and >30× improved *in vitro* clearance. Encouraged by this breakthrough finding, we incorporated the novel warhead across a wide array of P3−P2 combinations, where incorporation of a proline at P2 gave the early lead **4**, which retained much of the potency gained in the non-proline analog **3**. This lead also had far superior oral bioavailability in rodent and dog PK studies (Table 1), which was expected given the known ability of proline incorporation to enhance the exposure of orally administered peptidomimetics.[17] Aryl oxamide containing compounds (e.g., **3**) were unstable in rat/mouse plasma, so we used hamster as the rodent species for PK studies of such

https://doi.org/10.1021/acs.jmedchem.3c01938
J. Med. Chem. 2024, 67, 2369−2378

Scheme 1. Synthesis of Clinical Candidate CMX990:[a] A) Synthesis of the Novel Trifluoromethoxymethyl Ketone Warhead Bearing P1 Unit (19) and B) Core Synthetic Route for CMX990

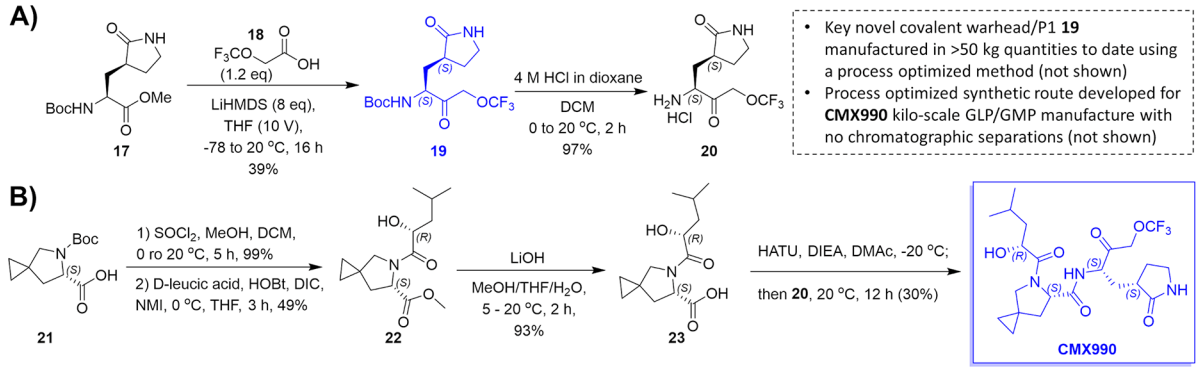

[a]The novel warhead-containing P1 fragment (**19**) can be manufactured at multi-kilogram scales at >98% purity and stored long-term. The **CMX990** manufactured using this process is a white crystalline solid, readily amenable for suspension formulation development as well as solid dosage form development.

Table 2. Comparative Performance of Clinical Candidate CMX990[a] vs Nirmatrelvir

	Nirmatrelvir	***CMX990***
***In Vitro* Potency**		
SARS-CoV-2 M^{pro} IC_{50} [nM]	28.1	23.4
HeLa-ACE2 CoV-2 $EC_{50/90}$ [nM]	70/148	37/90
ALI-HBEC CoV-2 $EC_{50/90}$ [nM]	25.3/44.8	5.3/9.6
HCT-8 hCoV-OC43 $EC_{50/90}$ [nM]	112/418	135/712
MCR5 hCoV-229E $EC_{50/90}$ [nM]	353/798	25/146
HeLa-ACE2 CoV-2 variants EC_{90} [nM], alpha/delta/omicron	242/196/117	63/35/37
Uninfected cytotoxicity CC_{50} [μM], HeLa-ACE2/HCT-8/MRC5/ALI-HBEC	>40/>30/>30/>3.3	>40/>30/>30/>3.3
ADME Properties [Mu/Rat/Dog/Cyno/Human]		
Microsomal/hepatocyte stability [CL_{int}, μL/min/mg; CL_{hep}, μL/min/10^6]	32.8/2.3 (human)	7.5/0.2 (human)
Human plasma stability [% at 2 h]	>80%	>80%
PPB [%]	73.6/58.6/98.8/70.3/54.8	48.1/88.8/63.6/62.3/56.3
Microsomal protein binding [%]	24.0/17.6/9.8/21.7/16.5	22.6/23.2/24.5/18.0/19.1
B/P ratio	0.67/0.85/0.67/0.83/1.12	0.89/0.94/0.74/0.88/1.15
$P_{app(a\rightarrow b/b\rightarrow a)}$ Caco-2 [10^{-6} cm/s]	0.9/9.0	0.6/9.3
Aqueous solubility	n.d.	1.4−1.5 mg/mL
***In Vivo* Properties[a] [Mu/Rat/Dog/Cyno]**		
Plasma clearance IV PK CL_p [mL/min/kg]	35.8/33.5/1.9/30.0	125/26.3/16.5/32.9
IV PK V_{ss} [L/kg]	2.0 (Vd)/1.0/0.57/1.5	1.2/2.7/1.1/1.2
F_{PO} (%)	17/44/69/3	14/12/53/1
Target Selectivity and Tox Profiling		
CEREP screen (10 μM, 44 targets)	No hits	No hits
hERG channel (CHO cells) IC_{50}	>10 μM	>10 μM
CYP inhibition IC_{50} (1A2, 2C19, 2C9, 2D6, 3A4)	3A4 = 46.4 μM, rest >50 μM	>50 μM (all)
Ames and MNT assay	Negative	Negative
Human peptidase selectivity panel, Cathepsin B/K/L/L2/S IC_{50} (μM)	No significant engagement except below cathepsins	
	>30/1.2/>30/14.6/1.8	4.3/0.10/1.6/0.2/0.7

[a]Further detailed *in vivo* data for **CMX990** in Table 3. n.d.= not determined.

analogs (Table 1). Despite the early interest, we discontinued development of **4** and other aniline oxamide leads due to a drug-related mutagenicity response seen in Ames assessments.

Switching to alkyl oxamides immediately alleviated the Ames assay outcome (e.g., **5**), indicating a clear link to the aniline oxamides regarding the positive Ames signal. Additionally, moving away from the aryl oxamides helped improve the human microsomal stability, which along with further SAR of P2 proline yielded the early lead **6** that performed similarly to nirmatrelvir in many aspects (Figure 2, Table 1), including a mouse efficacy study (data not disclosed at this time).

The alkyl oxamide derivative **6** had a very favorable outlook across broad safety profiling, including a peptidase panel assessment for cross reactivity with human proteases. However,

https://doi.org/10.1021/acs.jmedchem.3c01938
J. Med. Chem. 2024, 67, 2369−2378

at this time, nirmatrelvir was already available for treatment of SARS-CoV-2, and we did not see enough differentiation from nirmatrelvir potency nor clearance profiles to have sufficient justification to advance **6** for further development. This led us to further screen P2 prolines and P3 substituents that culminated in the discovery of the clinical candidate **CMX990** (Figure 2, Scheme 1), which featured an α-hydroxy acid P2-cap and a 4-spiro-cyclopropyl proline at P2. Potential (though not observed in later *in vitro* met-ID studies) byproducts (e.g., **7** and **8**; Table 1) of manufacturing and/or metabolism of **CMX990** were characterized as well, and these retained good potency and target engagement. Alternative P3 caps screened included other forms of α-hydroxy acids such as **9**, as well as P3 truncated analogs such as **10** (Table 1). These modifications either compromised potency or had worse *in vivo* clearance. In addition to the non-proline P2 analogs in Figure 2, additional exciting analogs that were pursued at the time included some non-aniline-oxamide P3 compounds (e.g., **11** and **12**), oxamide isostere derivatives such as **13**, and tetrahydrofuran P2-cap derivative **14** (Table 1). These had good potency (EC_{90} = 23−62 nM) in HeLa-ACE2 SARS-CoV-2 assays, though **14** had a less convincing biochemical IC_{50} (>60 nM) for target engagement. Alternative warheads, such as hydroxylmethyl ketones did have advantages in clearance (2× improved HLM-Cl_{int} in **15** vs **3**; Table 1) but lacked the desired potency profile (**15** HeLa-ACE2 CoV-2 EC_{90} = 245 nM, and CoV-2 M^{pro} IC_{50} = 160 nM; Table 1).

CMX990 had an excellent balance of physicochemical and ADME (absorption, digestion, metabolism, and excretion) properties, allowing for high potency in target engagement as well as favorable PK properties (Tables 1−3). It is a neutral molecule ($logD_{7.4}$ = 1.17), with a molecular weight of 491.5 g/mol, and pH-independent good aqueous solubility, with solubility of ∼1.4−1.5 mg/mL in buffers ranging from pH 1.2 to 7.4. In the presence of artificial intestinal fluids near neutral pH, lower solubility was observed in fed state simulated intestinal fluid (FeSSIF) (0.734 mg/mL, pH 5.0), with higher values observed in fasted state simulated intestinal fluid (FaSSIF) (>2 mg/mL, pH 6.5).

The synthetic route to clinical candidate **CMX990** is illustrated in Scheme 1, which is also representative of the assembly of other leads with the same warhead discussed in this report. The key starting reagents are commercially available P1-ester (also used in the syntheses of analogous compounds such as nirmatrelvir) **17**, trifluoromethylacetic acid **18**, D-leucic acid, and Boc-protected proline **21**. Alternative proline leads, such as **16** (Table 2) with a similar favorable potency/PK profile, were also considered for development. But the ease of access to **21** was significantly better (easily manufactured from hydroxyproline) versus these alternatives, making **CMX990** the ideal choice to progress with plans for eventual commercial-scale manufacture. The novel warhead-bearing P1 amino acid was synthesized starting with ester **17** (Scheme 1, panel A). Trifluoromethoxyacetic acid (**18**) is used as the key reagent to install the novel warhead on the BocNH-P1-ester **17**, yielding **19** at 47% yield. Boc deprotection of **19** with hydrochloric acid yielded salt **20**. Using this key intermediate, **CMX990** was assembled in four linear steps starting from Boc-proline **21** (Scheme 1, panel B). Following protecting group manipulation (99% yield), the proline was coupled with D-leucic acid (purchased commercially or synthesized in-house by conversion of D-leucine using literature methods[18] to yield **22** (49%), which was hydrolyzed under basic conditions to give the key carboxylic acid derivative **23**, in 93% yield. Thus obtained **23** was coupled under conventional peptide coupling conditions with the amine **20**, to give **CMX990** as a white crystalline solid. The described process has been used to make **19** and **CMX990** in >30 g scale. Further process optimization led to the manufacture of both **19** (>50 kg) and **CMX990** (>4 kg per batch) under conditions requiring no chromatographic separations (not shown in this disclosure).

The drug substance **CMX990** is stable for >1 year at room temperature storage. It is crystalline in nature, and the structure was unambiguously assigned by X-ray crystallography (Figure 3) using starting material stereochemistries that are

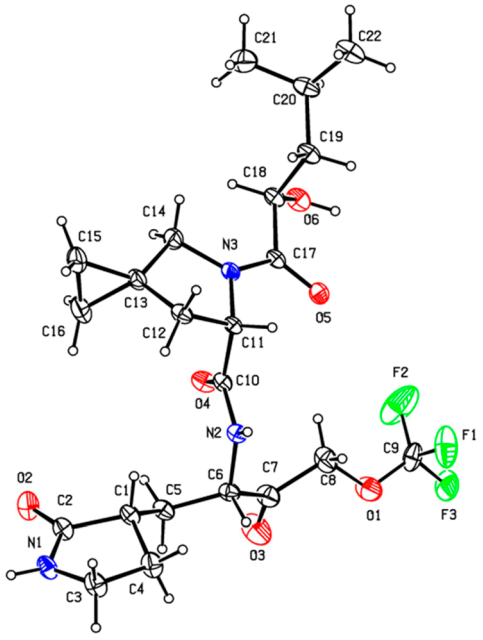

Figure 3. X-ray crystal structure of CMX990. CCDC deposition 2301255. Displacement ellipsoids are drawn at the 30% probability level.

unlikely to invert during synthesis. PXRD (not shown) remains consistent during mechanical handling (such as micronization), and the material was readily amenable for the development of both simple aqueous suspension (e.g., in 0.5% methyl cellulose) or solid dosage forms. The stereochemistry of all four chiral centers of **CMX990** (C1, C6, C11, and C18; Figure 3) was found to be important for the best activity, as confirmed with the synthesis (not shown) of all 16 possible stereoisomers of **CMX990**. P1-epimerization (Figure 3 − at C6), often expected as the most likely to happen in a synthesis such as Scheme 1, led to >2× loss of potency (HeLa-ACE-2 CoV-2 EC_{90} = 234 nM, HLM-Cl_{int} = 11.3 μL/min/mg) without impacting microsomal clearance. Inversion of the P3-hydroxy group (Figure 3 − at C18, HeLa-ACE-2 CoV-2 EC_{90} = 196 nM, HLM-Cl_{int} = 23.7 μL/min/mg, $F_{PO(dog)}$ = 55%) or the pyrrolidinone stereocenter (Figure 3 − C1 epimer; HeLa-ACE-2 CoV-2 EC_{90} = 150 nM, HLM-Cl_{int} = 13.9 μL/min/mg) was least critical, with the proline stereochemistry being the most critical (Figure 3 − C11 epimer; HeLa-ACE-2 CoV-2 EC_{90} = 6 μM, HLM-Cl_{int} = 31.0 μL/min/mg). Given the importance of ensuring chiral purity, significant effort was taken in developing manufacturing processes for **CMX990** to mitigate epimerization as well as to establish appropriate

https://doi.org/10.1021/acs.jmedchem.3c01938
J. Med. Chem. 2024, 67, 2369−2378

Table 3. Pharmacokinetic Parameters of CMX990 Following a Single IV or PO Administration in Solution Formulation[a]

	Mouse	Rat	Cyno Monkey	Dog
IV				
CL (mL/min/kg)	125 ± 18	26.3 ± 6.58	32.9 ± 6.5	16.5 ± 3.2
V_{ss} (L/kg)	1.23 ± 0.17	2.69 ± 0.93	1.19 ± 0.16	1.11 ± 0.14
MRT (h)	0.17 ± 0.02	1.67 ± 0.19	0.61 ± 0.04	0.94
PO				
T_{max} (h)	0.5	0.67 ± 0.29	0.83 ± 0.29	0.83 ± 0.29
DN C_{max} (ng/mL)	19.0 ± 12.3	27.6 ± 8.7	2.4 ± 1.5	183.3 ± 45.0
DN AUC_{0-inf} (ng*h/mL)	19.7 ± 4.2	81.3 ± 17.9	5.5 ± 2.9	472.5 ± 38.9
F (%)	14.5 ± 3.1	12.2 ± 2.7	1.1 ± 0.55	52.8 ± 3.7

[a]Solution formulation = EtOH/PEG300/water (1:4:5 v/v). All IV administrations at 2 mg/kg. Mouse and rat PO administrations at 30 mg/kg; cyno and dog PO administrations at 10 mg/kg. AUC = area under the curve, CL = clearance, C_{max} = maximum concentration, DN = dose normalized, F = % bioavailability, MRT = mean residence time, T_{max} = time to maximum concentration, V_{ss} = steady-state volume of distribution.

purification methods (particularly using alternative dissolution profiles/recrystallization).

Target engagement of **CMX990** was validated in a biochemical assay for SARS-CoV-2 M^{pro}, where it was demonstrated that the compound engages the enzyme as a reversible inhibitor (IC_{50} = 23.4 nM, Table 2). The reversible/irreversible character of the compound was assessed via different pre-incubation times of the inhibitor and the enzyme. In general, an irreversible inhibitor will increase its capacity to block the enzyme with increasingly longer incubation times in the presence of the enzyme prior to addition of substrate. Conversely, a constant IC_{50} supports a reversible mechanism.[19] Within the same assay, compound **3** (same warhead) was found to be a reversible inhibitor, while an analogous compound to **2** (aryloxymethyl ketone warhead) was found to be an irreversibly covalent inhibitor. Additional experiments are ongoing to further define the reversible/irreversible nature of the warhead; via co-crystal structure generation, NMR-based studies, as well as elaborate enzymology experiments to explore Michaelis−Menten kinetics.

CMX990 was also screened in a pan-coronavirus reporter assay panel (data not shown), demonstrating the ability to potently inhibit up to 20 coronaviral protease types/variants including P132H (omicron), MERS, and HKU1 (human) but not the negative control flavivirus system (ZIKV, no inhibition).

The *in vitro* activity of **CMX990** in a HeLa-ACE2 cell culture model of SARS-CoV-2 infection provided a mean antiviral $EC_{50/90}$ of 37/90 nM, with no detectable cytotoxicity observed (CC_{50} > 40 μM). **CMX990** potently and reproducibly inhibited the replication of eight SARS-CoV-2 variants tested, including alpha, delta, and omicron (Table 2).

It also showed activity versus other betacoronaviruses (e.g., HCoV-OC43) as well as alphacoronaviruses (e.g., HCoV-229E) in live virus assays, corroborating the findings in reporter assay data to designate **CMX990** as a pan-coronavirus inhibitor. As a more physiologically relevant model, SARS-CoV-2 replication was measured in normal primary human bronchial epithelial cells (HBECs). Air−liquid interface (ALI) cultures of HBECs recapitulate key properties of the airway epithelium, including cell polarization, mucus secretion, and cilia beating. **CMX990** performed 5× superior to nirmatrelvir in ALI-HBECs with a $EC_{50/90}$ = 5.3/9.6 nM, having up to a 3-log reduction in viral load (72 h post-infection) when treated at 370 nM. No cytotoxicity was detected in any of these cell-based models.

CMX990 has low to moderate plasma protein binding across species over the range 0.5−20 μM as determined by equilibrium dialysis (Table 2). No meaningful concentration differences (i.e., >2-fold) in protein binding were observed in mouse, dog, monkey, and human plasma, with a concentration-dependent decrease in protein binding noted in rat at 20 μM. No meaningful species differences in protein binding were observed between species at 20 μM. The protein binding in human was comparable to mouse and dog, the two species selected for toxicity studies. **CMX990** (1 μM) had mean blood-to-plasma ratios (B/P) of 0.89, 0.94, 0.74, 0.88, and 1.15 in mouse, rat, dog, monkey, and human, respectively, suggesting no preferential partitioning into red blood cells in these species.

Metabolic turnover of **CMX990** was low in rat, dog, and human, with a more rapid metabolism in mouse and monkey (Table 2). In microsomal stability studies conducted in the presence or absence of selective CYP450 inhibitors and in stability studies with individual recombinant CYP isozymes (CYP1A2, 2B6, 2C8, 2C9, 2C19, 2D6, and 3A4), CYP3A4 was identified as the only enzyme contributing to the metabolism of **CMX990**. Excretion of the drug is anticipated to happen via both bile and urine. The route of elimination of **CMX990** was evaluated in bile duct cannulated rats. Following a single 3 mg/kg intravenous bolus dose, plasma, urine, and bile samples were collected up to 24 h post-dose. The plasma half-life was short, most of the drug was eliminated by 7 h post-dose, and ∼6.7% and 7.5% of unchanged **CMX990** was excreted to bile and urine, respectively. These data suggested that multiple clearance mechanisms are involved in the elimination of **CMX990**.

No critical off-target safety concerns were found for **CMX990** in a CEREP panel screen (Eurofins, 44 pharmacological targets, no individual target inhibition ≥50% at 10 μM concentration) or in a cardiac panel screen (including Nav1.5, Cav1.2, hERG). Peptidase panel inhibition data (Eurofins, at 10 μM) revealed no significant engagement of critical human peptidases (including calpain-1, caspases, chymase, chymotrypsin, DPP4, elastase 2, plasma Kallikrein, and plasmin), except for some cathepsin isoforms. Some extent of *in vitro* cathepsin inhibition is observed in many of the comparative SARS-CoV-2 peptidomimetic inhibitors we have studied to date including nirmatrelvir. Genotoxicity and mutagenicity concerns were also excluded via negative micronucleus test (MNT) and Ames assay data (Table 2). Direct and time-dependent inhibition potential of **CMX990** on CYP1A2,

https://doi.org/10.1021/acs.jmedchem.3c01938
J. Med. Chem. 2024, 67, 2369−2378

CYP2C9, CYP2C19, CYP2D6, and CYP3A4 was investigated in human liver microsomes, where **CMX990** did not inhibit these major CYP isoforms (IC_{50} > 50 μM). There was no apparent shift in CYP3A4 IC_{50} (>50 μM) with a 30 min pre-incubation, indicating **CMX990** is not a time-dependent inhibitor of CYP3A4.

CMX990's PK profile was characterized by moderate plasma clearance values in dog and rat, with higher clearance in monkey and mouse, following 2 mg/kg intravenous doses (Table 3). The steady-state volume of distribution was moderate in all species (V_{ss} = 1.0−2.3 L/kg). Plasma elimination half-life after IV dosing for **CMX990** was <1 h in both mouse and monkey, with values of 1.2−1.9 and 2.0 h in rat and dog, respectively. The compound was rapidly absorbed, with T_{max} values ranging between 0.33 to 1.7 h across species. Oral bioavailability was low in monkey (1%), moderate in mouse and rat (14−22%), and high in dog (53%; Table 3), which was similar to the preclinical profile seen for nirmatrelvir in comparative in-house studies (Table 2). Low oral bioavailability in monkey for such peptidomimetics has been presented in prior literature.[20] *In vivo* hepatic clearance predicted from *in vitro* intrinsic clearance (using scaling factors and well-stirred liver model) showed good correlation with measured *in vivo* clearance trends in preclinical animals (Tables 2 and 3).

Based on this excellent *in vitro*-to-*in vivo* correlation (IVIVc) of clearance from other species, human clearance for **CMX990** was predicted to be very low (predicted CL_h <5.9 [microsomal], <3.0 [hepatocytes]). This led to human-equivalent dose projections (oral, <500 mg/day) of once or twice a day with no ritonavir boost required to cover efficacious C_{trough} exposure, significantly differentiating **CMX990** from nirmatrelvir. A ritonavir boosted study (not shown) done in dogs showed no significant advantage toward the PK profile of **CMX990** versus monotherapy.

Multiple mono-, di-, and tri-oxidative metabolites were identified (not shown) following incubations in microsomes (8 metabolites) and hepatocytes (15 metabolites) across species. No human unique metabolites were identified in either microsome or hepatocyte incubations, and all human metabolites were present in the species selected for toxicology studies (e.g., mouse, dog, or both). The intended clinical route of administration for **CMX990** was decided to be oral administration; therefore, all of the toxicology studies were conducted by oral gavage.

Several additional studies (not shown) explored the effects of formulation, dose, and dosing frequency on **CMX990** exposures following oral administration in CD-1 mice and beagle dogs. In mice, dose-normalized AUC values were comparable between the 30 mg/kg solution formulation and the 35, 50, 100, 300, and 500 mg/kg BID doses of a suspension of micronized API (active pharmaceutic ingredient), with greater dose proportional values following the 50 mg/kg BID dose. In dogs, exposures from aqueous suspensions of micronized API (D_{90} < 50 μM) were higher than those obtained from aqueous suspensions of non-micronized drug, with BID dosing providing greater than proportional increases in AUC when compared to the same single daily dose. Taken together, BID dosing of the micronized API as a suspension in 0.5% methylcellulose (MC) was selected as the formulation for repeat-dose toxicology studies.

The general toxicity profile of **CMX990** was assessed in CD-1 mice and beagle dogs. **CMX990** was administered by oral gavage to CD-1 mice and beagle dogs at dosages of up to 1000 mg/kg/day (500 mg/kg/dose, BID, 8 h apart) for 5 days with a 14-day recovery period. **CMX990** was well-tolerated in both species. In mice, non-adverse microscopic findings only included sporadic **CMX990**-related minimal to mild increased single-cell necrosis of hepatocytes without associated changes in serum liver enzymes. In dogs, the liver was the primary target organ, with microscopic findings of adverse centrilobular hepatocellular degeneration/necrosis that was accompanied by increases in serum liver enzymes. Additional non-adverse findings in dog also included epithelial single-cell necrosis and mononuclear cell infiltration in gall bladder, decreased cellularity in thymus, decreases in reticulocytes, and increases in clotting times. These findings were generally monitorable and either completely reversible or were in the process of resolution (liver) at the end of the recovery phase. The no observed adverse effect levels (NOAELs) in mice and dogs are considered to be 1000 mg/kg/day (500 mg/kg/dose, BID) and 150 mg/kg/day (75 mg/kg/dose, BID), respectively, for 5-day administration.

CONCLUSION

Inhibition of the highly conserved viral main protease (M^{pro}) is one of the best accepted means to develop antivirals to coronaviruses. SARS-CoV-2 M^{pro} has been well validated as a target with an FDA-approved drug now on the market, as well as from a large body of research that has evolved over the past three years. Currently available therapies for SARS-CoV-2 infection have an array of disadvantages, including DDI and other toxicology concerns, global accessibility, and suboptimal potencies of target engagement. Particularly in the view of future pandemic preparedness, it is imperative that further improvements are made to develop better and/or alternative pharmaceuticals that can tackle this drug target, which has no human homolog. The key breakthrough of the described program to address this need was based on a unique unprecedented cysteine-protease-engaging warhead that enabled low nanomolar antiviral potencies.

CMX990 features a novel covalent warhead, excellent antiviral properties (SARS-CoV-2 EC_{90} [ALI-HBEC] = 10 nM), good oral bioavailability and tolerability in preclinical species, and excellent human *in vitro* metabolic clearance (Pred. CL_h < 6 mL/min/kg), and HED predictions (once or twice a day dosing) supporting unboosted oral therapy. With this promising background and the support of a large multidisciplinary team, **CMX990** progressed to a Phase 1 clinical trial in ∼10 months after its first synthesis.

EXPERIMENTAL SECTION

Materials and Methods. All reagents and solvents were purchased from commercial sources and used without further purification. Flash column chromatography was performed using silica gel (200−300 mesh). All reactions were monitored by TLC (pre-coated EMD silica gel 60 F254 TLC aluminum sheets and visualized with a UV lamp or appropriate stains) and/or LCMS (Waters Acquity UPLC system, 2 or 4 min run of a 10−90% mobile phase gradient of acetonitrile in water [+0.1% formic acid]). NMR spectra were obtained on Bruker AV400 or AV500 instruments, and data was analyzed using the MestReNova NMR software (Mestrelab Research S. L.). Chemical shifts (δ) are expressed in ppm and are internally referenced for ^{1}H NMR (DMSO-d_6 2.50 ppm) and ^{13}C NMR ($CDCl_3$ 77.16 ppm, DMSO-d_6 39.52 ppm). X-ray data was collected at room temperature on a Bruker D8 QUEST instrument

https://doi.org/10.1021/acs.jmedchem.3c01938
J. Med. Chem. 2024, 67, 2369−2378

with an IμS Mo microfocus source (λ = 0.7107 Å) and a PHOTON-III detector.

NMR spectra for the final proline-containing derivatives commonly exist as rotamer populations in DMSO-d_6. The activated ketone in the novel warhead creates a transient reversible-equilibrium under acid modified (e.g., TFA, formic acid) aqueous chromatography conditions, as represented by the appearance of a leading non-baseline separated second (minor) peak in the chromatogram. Occasionally, some compounds (e.g., compound **10** with truncated P2-cap) also show similar interactions/equilibrium in NMR, including interactions of the P2-proline nitrogen with the warhead ketone. The isolation of individual components of these non-baseline separated material, and re-injection results in the same equilibrium appearance. Hence, when doing chromatographic separations under reversed-phase conditions containing acidic modifiers, the entirety of this peak (leading minor-peak + the later-eluting major peak) should be isolated as a single peak. Alternatively, reversed-phase separation can be carried out without the presence of an acidic modifier, with a slight compromise on sharpness of the peak.

Chemistry. All compounds with the novel trifluoromethoxymethyl warhead were synthesized according to the representative procedure outlined for **CMX990** below. All compounds are >95% pure by HPLC and/or NMR analyses.

***tert*-Butyl ((*S*)-3-oxo-1-((*S*)-2-oxopyrrolidin-3-yl)-4-(trifluoromethoxy)butan-2-yl)carbamate (19).** To a stirred solution of 2-(trifluoromethoxy)acetic acid **18** (8.45 g, 58.67 mmol, 1.2 equiv) in THF (90 mL), lithium bis(trimethylsilyl)amide solution (1 M in THF, 391.16 mL, 391.16 mmol, 8.1 equiv) was added, and the resulting mixture was stirred at −78 °C for 1 h. Methyl (*S*)-2-((*tert*-butoxycarbonyl)amino)-3-((*S*)-2-oxopyrrolidin-3-yl)-propanoate (**17**) (14.0 g, 48.89 mmol, 1.0 equiv) in THF (50 mL) was slowly added to the reaction mixture at −78 °C and the reaction mixture was stirred at −78 °C for 3 h and then at room temperature for 16 h. After completion of the reaction, the reaction mixture was quenched with AcOH (28 mL) in THF (126 mL) at 0 °C and diluted with water (500 mL). The resulting mixture was filtered through Celite and washed with EtOAc (500 mL), and filtrate was extracted with EtOAc (3 × 500 mL). The combined organic layer was dried over anhydrous Na_2SO_4, filtered, and evaporated under reduced pressure to get crude compound. The resulting crude compound was purified by davisil grade silica gel column chromatography using 20% ethyl acetate in hexane as the eluent to afford *tert*-butyl ((*S*)-3-oxo-1-((*S*)-2-oxopyrrolidin-3-yl)-4-(trifluoromethoxy)butan-2-yl)carbamate (**19**, 6.79 g, 19.2 mmol, 39%) as a pale brown solid. [*TLC system*: EtOAc: pet-ether (7:3); R_f value: 0.4]. LCMS *m*/*z* 355.37 (M+1); ^{1}H NMR (400 MHz, DMSO-d_6) δ 7.66 (s, 1H), 7.52 (dd, *J* = 7.2 Hz, 18 Hz, 1H), 4.98 (s, 2H), 4.15−4.09 (m, 1H), 3.19−3.12 (m, 2H), 2.50−2.13 (m, 2H), 1.91−1.84 (m, 1H), 1.68−1.57 (m, 2H), 1.39 (s, 9H).

(3*S*)-3-[(2*S*)-2-Amino-3-oxo-4-(trifluoromethoxy)butyl]-pyrrolidin-2-one hydrochloride (20). To a stirred solution of *tert*-butyl *N*-[(2*S*)-3-oxo-1-[(3*S*)-2-oxopyrrolidin-3-yl]-4-(trifluoromethoxy)butan-2-yl]carbamate (**19**; 20 g, 56.5 mmol, 1.0 equiv) in DCM (300 mL) was added HCl (4 M in dioxane, 34.30 mL, 20 equiv) dropwise at 0 °C under nitrogen atmosphere. The resulting mixture was stirred for additional 1h at room temperature. The resulting mixture was concentrated under reduced pressure. The residue was purified by trituration with Et_2O (150 mL) to afford (3*S*)-3-[(2*S*)-2-amino-3-oxo-4-(trifluoromethoxy)butyl]pyrrolidin-2-one hydrochloride as an off-white solid (**20**; 16 g, 55.0 mmol, 97% yield). LCMS *m*/*z* = 255 (M+1).

Methyl (*S*)-5-((*R*)-2-hydroxy-4-methylpentanoyl)-5-azaspiro [2.4] heptane-6-carboxylate (22). To a stirred solution of the starting proline **21** (150 g, 622 mmol, 1.0 equiv) in MeOH (2 L) was slowly added $SOCl_2$ (221.86 g, 1.86 mol, 3 equiv) and DMF (1.36 g, 18.65 mmol, 0.03 equiv) dropwise at 0 °C under a nitrogen atmosphere. The resulting mixture was stirred for 5 h at room temperature. After the reaction was completed, the mixture was concentrated under reduced pressure to afford methyl (*S*)-5-azaspiro [2.4] heptane-6-carboxylate hydrochloride (120 g, 615 mmol, 99%) as a light-yellow oil.

To a stirred mixture of methyl (*S*)-5-azaspiro [2.4] heptane-6-carboxylate hydrochloride (100 g, 522 mmol, 1.0 equiv) and (*R*)-2-hydroxy-4-methylpentanoic acid (75.85 g, 574 mmol, 1.1 equiv) in THF (3 L) were slowly added DIC (79.02 g, 626 mmol, 1.2 equiv) and 1-methyl-1*H*-imidazole (171.36 g, 2.09 mol, 4 equiv) in portions at 0 °C. The resulting mixture was stirred for 10 min at 0 °C. Then a solution of HOBt (84.61 g, 626 mmol, 1.2 equiv) in THF (200 mL) was slowly added dropwise over 30 min. The resulting mixture was stirred for 3 h at 0 °C and filtered, and the filtrate was concentrated under reduced pressure. This residue was purified by silica gel column chromatography and eluted with PE:THF (5:1), to afford partially pure **22** (69 g, 256 mmol, 49%) as a white solid (with intramolecularly trans-esterified compound as an impurity).

(*S*)-5-((*R*)-2-Hydroxy-4-methylpentanoyl)-5-azaspiro[2.4]-heptane-6-carboxylic acid (23). A solution of **22** (69 g, 256 mmol, 1.0 equiv) in THF (700 mL) was stirred at 0 °C. LiOH (7.36 g, 307 mmol, 1.2 equiv) in H_2O (200 mL) was added to this dropwise over 20 min while maintaining the reaction mixture temperature at 0 °C. The resulting mixture was stirred for 3 h at room temperature, acidified to pH = 3 with 50 mL of HCl (6 N) at 0 °C, and then extracted with EtOAc (3 × 500 mL). The combined organic layers were washed with brine (250 mL), dried over 250 g of anhydrous Na_2SO_4, filtered, and concentrated *in vacuo* to afford **23** (61 g, 239 mmol, 93%) as a white solid.

(*S*)-5-((*R*)-2-Hydroxy-4-methylpentanoyl)-*N*-((*S*)-3-oxo-1-((*S*)-2-oxopyrrolidin-3-yl)-4-(trifluoromethoxy)butan-2-yl)-5-azaspiro[2.4]heptane-6-carboxamide (CMX990). To a stirred solution of acid **23** (61 g, 239 mmol, 1.0 equiv) and amine hydrochloride **20** (85.97 g, 263 mmol, 1.1 equiv) in DMA (1.2 L) was added HATU (109.02 g, 287 mmol, 1.2 equiv). The mixture was stirred for 10 min at −20 °C in an ethanol-ice bath, and DIPEA (123.52 g, 956 mmol, 4.0 equiv) diluted with 250 mL of DMA was slowly added. The resulting mixture was stirred for 12 h at room temperature, then diluted with water (1.5 L), and extracted with EtOAc (2 × 2.0 L). The combined organic layers were washed with brine (500 mL), dried over with anhydrous Na_2SO_4, filtered, and concentrated *in vacuo*. The residue was taken up in EtOAc (500 mL) and washed with 1 M hydrochloric acid (3 × 250 mL). The water layers were extracted with EtOAc (2 × 500 mL), combined organic layers dried over anhydrous Na_2SO_4, filtered, and concentrated *in vacuo*. The resultant residue was purified by silica gel column chromatography, eluted with PE:THF = 1:1 to afford 27 g (SFC: 94% purity, batch A) and 19 g (SFC: 91% purity, batch B) **CMX990**. 19 g (SFC: 91% purity, batch B) was purified by SFC to give 12 g material (SFC: 98% purity, batch C). Batch A and C were combined and slurried with Et_2O (400 mL) to give **CMX990** (35.8 g, 72.8 mmol, 30%) as a white crystalline solid.

SFC separation conditions: Column, CHIRAL ART Cellulose-SC, 3 × 25 cm, 5 μm; Mobile Phase A, CO_2; Mobile Phase B, IPA:MeCN = 1:1; Flow rate, 80 mL/min; Gradient, isocratic 25% B; Column Temperature (°C), 35; Back Pressure (bar), 100; detection wavelength, 220 nm; Sample Solvent, IPA:MeCN = 2:1; Injection Volume, 5 mL (×110 runs)

HRMS *m*/*z* calcd. for $C_{22}H_{33}F_3N_3O_6^+$ $[M + H]^+$ 492.2316, found 492.4428; ^{1}H NMR (400 MHz, DMSO-d_6) δ 8.67 (br d, *J* = 7.0 Hz, 0.2H), 8.43 (br d, *J* = 7.7 Hz, 0.7H), 7.73 (br s, 0.2H), 7.67 (br s, 0.7H), 5.10 (d, *J* = 7.3 Hz, 0.2H), 5.02 (d, *J* = 17.4 Hz, 1.2H, some overlap), 4.88 (d, *J* = 17.3 Hz, 1H), 4.60 (d, *J* = 7.3 Hz, 0.7H), 4.35 (m, 1.8H), 4.11 (m, 0.8H), 3.91 (m, 0.2H), 3.58−3.46 (m, 1.8H), 3.22−3.06 (m, 2.2H), 2.30−2.06 (m, 3H), 2.03−1.89 (m, 1H), 1.84−1.54 (m, 4H), 1.51−1.18 (m, 2H), 0.88 (d, *J* = 6.8 Hz, 2.3H), 0.87 (d, *J* = 6.5 Hz, 2.3H), 0.88 (d, *J* = 6.7 Hz, 0.7H), 0.87 (d, *J* = 6.5 Hz, 0.7H), 0.66−0.37 (m, 4H); ^{19}F NMR (376 MHz, $CDCl_3$) δ −60.86; ^{13}C NMR (101 MHz, $CDCl_3$) δ 200.80, 180.44, 174.63, 172.76, 121.63 (q, *J* = 256.3 Hz), 69.04 (q, *J* = 2.9 Hz), 61.50, 56.41, 54.10, 43.17, 40.94, 38.76, 37.26, 31.28, 28.89, 24.62, 23.72, 21.65, 21.09, 13.69, 7.21, 1.13; Melting point = 170.2−172.6 °C; Anal. Calcd for

https://doi.org/10.1021/acs.jmedchem.3c01938
J. Med. Chem. 2024, 67, 2369−2378

$C_{22}H_{32}F_3N_3O_6$: C, 53.76; H, 6.56; N, 8.55 Found: C, 53.34; H, 6.60; N, 8.41.

■ ASSOCIATED CONTENT

Data Availability Statement

CCDC deposition 2301255 contains the supplementary crystallographic data for the CMX990 single-crystal structure. This data can be obtained free of charge by emailing data_request@ccdc.cam.ac.uk, or by contacting The Cambridge Crystallographic Data Centre, 12 Union Road, Cambridge CB2 1EZ, UK; fax: + 44 1223 336033.

Supporting Information

The Supporting Information is available free of charge at https://pubs.acs.org/doi/10.1021/acs.jmedchem.3c01938.

Additional synthetic procedures and characterization data including NMR spectra, *in vitro* assay information, and DMPK assay information (PDF)

Molecular strings (CSV)

■ AUTHOR INFORMATION

Corresponding Authors

Arnab K. Chatterjee − *Calibr at Scripps Research Institute, La Jolla, California 92037, United States;* orcid.org/0000-0001-5171-7982; Email: achatterjee@scripps.edu

N. G. R. Dayan Elshan − *Calibr at Scripps Research Institute, La Jolla, California 92037, United States*; Email: dnakath@scripps.edu

Authors

Karen C. Wolff − *Calibr at Scripps Research Institute, La Jolla, California 92037, United States*

Laura Riva − *Calibr at Scripps Research Institute, La Jolla, California 92037, United States*

Ashley K. Woods − *Calibr at Scripps Research Institute, La Jolla, California 92037, United States*

Gennadii Grabovyi − *Calibr at Scripps Research Institute, La Jolla, California 92037, United States;* orcid.org/0000-0001-8999-9532

Katy Wilson − *Calibr at Scripps Research Institute, La Jolla, California 92037, United States*

James Pedroarena − *Calibr at Scripps Research Institute, La Jolla, California 92037, United States*

Sourav Ghorai − *Calibr at Scripps Research Institute, La Jolla, California 92037, United States*

Armen Nazarian − *Calibr at Scripps Research Institute, La Jolla, California 92037, United States*

Frank Weiss − *Calibr at Scripps Research Institute, La Jolla, California 92037, United States*

Yuyin Liu − *Calibr at Scripps Research Institute, La Jolla, California 92037, United States*

Wrickban Mazumdar − *Calibr at Scripps Research Institute, La Jolla, California 92037, United States*

Lirui Song − *Calibr at Scripps Research Institute, La Jolla, California 92037, United States*

Neechi Okwor − *Calibr at Scripps Research Institute, La Jolla, California 92037, United States*

Jacqueline Malvin − *Calibr at Scripps Research Institute, La Jolla, California 92037, United States*

Malina A. Bakowski − *Calibr at Scripps Research Institute, La Jolla, California 92037, United States*

Nathan Beutler − *Department of Immunology and Microbiology, The Scripps Research Institute, La Jolla, California 92037, United States*

Melanie G. Kirkpatrick − *Calibr at Scripps Research Institute, La Jolla, California 92037, United States*

Amal Gebara-Lamb − *Calibr at Scripps Research Institute, La Jolla, California 92037, United States*

Edward Huang − *Calibr at Scripps Research Institute, La Jolla, California 92037, United States*

Vân T. B. Nguyen-Tran − *Calibr at Scripps Research Institute, La Jolla, California 92037, United States*

Victor Chi − *Calibr at Scripps Research Institute, La Jolla, California 92037, United States*

Shuangwei Li − *Calibr at Scripps Research Institute, La Jolla, California 92037, United States*

Thomas F. Rogers − *Department of Immunology and Microbiology, The Scripps Research Institute, La Jolla, California 92037, United States*

Case W. McNamara − *Calibr at Scripps Research Institute, La Jolla, California 92037, United States;* orcid.org/0000-0002-5754-3407

Anil Kumar Gupta − *Calibr at Scripps Research Institute, La Jolla, California 92037, United States;* orcid.org/0000-0001-5035-9597

Alireza Rahimi − *Calibr at Scripps Research Institute, La Jolla, California 92037, United States*

Jian Jeffrey Chen − *Calibr at Scripps Research Institute, La Jolla, California 92037, United States*

Sean B. Joseph − *Calibr at Scripps Research Institute, La Jolla, California 92037, United States;* orcid.org/0000-0002-2602-8517

Peter G. Schultz − *Calibr at Scripps Research Institute, La Jolla, California 92037, United States; Department of Chemistry, The Scripps Research Institute, La Jolla, California 92037, United States;* orcid.org/0000-0003-3188-1202

Complete contact information is available at: https://pubs.acs.org/10.1021/acs.jmedchem.3c01938

Notes

The authors declare no competing financial interest.

■ ACKNOWLEDGMENTS

This work was supported by grants from the Bill and Melinda Gates Foundation (INV-028691, COVID-19 CTA GPP). The authors would like to thank Sreehari Babu Putchakayala (Aragen Life Sciences) for assistance in formulations development work, Dr. Jason Chen and his team at the Scripps Research Automated Synthesis facility for assistance with chiral purifications/characterization, Calibr compound management team and administrative teams, Dr. Kit Bonin (Calibr) and Dr. Geneva Hargis (Calibr) for manuscript preparation assistance, and the diverse team of subject-matter-experts engaged by the Bill and Melinda Gates Foundation to guide and accelerate this program into Ph1 clinical studies.

■ ABBREVIATIONS USED

$3CL^{pro}$, 3C-like protease; ACE-2, angiotensin-converting enzyme-2; ALI, air−liquid interface; CL, clearance; CLhep, clearance in hepatocytes; Cl_{int}, intrinsic clearance; Cl_p, plasma clearance; CL^{pro}, 3C-like protease; C_{max}, maximum concentration; C_{trough}, concentration before next dose; *F*, bioavail-

https://doi.org/10.1021/acs.jmedchem.3c01938
J. Med. Chem. 2024, 67, 2369−2378

ability; DN, dose normalized; HBEC, human bronchial epithelial cells; HED, human equivalent dose; HKU1, human coronavirus 1; HLM, human liver microsomes; hPPB, human plasma protein binding; IVIVc, *in vitro*-to-*in vivo* correlation; logD, logarithm of partition coefficient for ionizable compounds; MC, methylcellulose; MERS, Middle Eastern respiratory syndrome; met-ID, metabolite identification; MNT, micronucleus; M^{pro}, main protease (i.e., $3CL^{pro}$); MRT, mean residence time; Mu, mouse; n.c., not calculated; n.d., not determined; P1, amino acid 1, recognition element with a lactam side chain; P132H, omicron variant of SARS-CoV-2; P2, amino acid 2; P3, a N-Cap or amino acid 3; P_{app}, apparent permeability coefficient; PL^{pro}, papain-like protease; ReFRAME, Repurposing, Focused Rescue, and Accelerated MEdchem library; SARS-CoV-2, severe acute respiratory syndrome coronavirus 2; T_{max}, time to peak drug concentration; V_{ss}, steady-state volume of distribution; WH, warhead; ZIKV, Zika virus

REFERENCES

(1) World Health Organization, *WHO COVID-19 Dashboard*, https://covid19.who.int/ (accessed September, 27, 2023).

(2) Yadav, T.; Kumar, S.; Mishra, G.; Saxena, S. K. Tracking the COVID-19 vaccines: The global landscape. *Hum. Vaccin. Immunother.* **2023**, *19* (1), 2191577.

(3) Gilead, *Veklury home page*, https://www.veklury.com/ (accessed September 27, 2023).

(4) Pfizer, *Paxlovid home page*, https://www.paxlovid.com/ (accessed September 27, 2023).

(5) Shionogi, *Xocova home page*, https://www.shionogi.com/global/en/news/2023/04/20230404.html (accessed September 27, 2023).

(6) Cox, R. M.; Wolf, J. D.; Plemper, R. K. Therapeutically administered ribonucleoside analogue MK-4482/EIDD-2801 blocks SARS-CoV-2 transmission in ferrets. *Nat. Microbiol.* **2021**, *6* (1), 11−18.

(7) Jiang, X.; Su, H.; Shang, W.; Zhou, F.; Zhang, Y.; Zhao, W.; Zhang, Q.; Xie, H.; Jiang, L.; Nie, T.; et al. Structure-based development and preclinical evaluation of the SARS-CoV-2 3C-like protease inhibitor simnotrelvir. *Nat. Commun.* **2023**, *14* (1), 6463.

(8) Janes, J.; Young, M. E.; Chen, E.; Rogers, N. H.; Burgstaller-Muehlbacher, S.; Hughes, L. D.; Love, M. S.; Hull, M. V.; Kuhen, K. L.; Woods, A. K.; et al. The ReFRAME library as a comprehensive drug repurposing library and its application to the treatment of cryptosporidiosis. *Proc. Natl. Acad. Sci. U. S. A.* **2018**, *115* (42), 10750−10755.

(9) Bafna, K.; Cioffi, C. L.; Krug, R. M.; Montelione, G. T. Structural similarities between SARS-CoV2 3CL(pro) and other viral proteases suggest potential lead molecules for developing broad spectrum antivirals. *Front. Chem.* **2022**, *10*, 948553.

(10) Chen, Y.; Liu, Q.; Guo, D. Emerging coronaviruses: Genome structure, replication, and pathogenesis. *J. Med. Virol.* **2020**, *92* (4), 418−423.

(11) Hilgenfeld, R. From SARS to MERS: crystallographic studies on coronaviral proteases enable antiviral drug design. *FEBS J.* **2014**, *281* (18), 4085−4096.

(12) Zhang, L.; Lin, D.; Kusov, Y.; Nian, Y.; Ma, Q.; Wang, J.; von Brunn, A.; Leyssen, P.; Lanko, K.; Neyts, J.; et al. alpha-Ketoamides as Broad-Spectrum Inhibitors of Coronavirus and Enterovirus Replication: Structure-Based Design, Synthesis, and Activity Assessment. *J. Med. Chem.* **2020**, *63* (9), 4562−4578.

(13) Dai, W.; Zhang, B.; Jiang, X. M.; Su, H.; Li, J.; Zhao, Y.; Xie, X.; Jin, Z.; Peng, J.; Liu, F.; et al. Structure-based design of antiviral drug candidates targeting the SARS-CoV-2 main protease. *Science* **2020**, *368* (6497), 1331−1335.

(14) Dragovich, P. S.; Prins, T. J.; Zhou, R.; Webber, S. E.; Marakovits, J. T.; Fuhrman, S. A.; Patick, A. K.; Matthews, D. A.; Lee, C. A.; Ford, C. E.; et al. Structure-based design, synthesis, and biological evaluation of irreversible human rhinovirus 3C protease inhibitors. 4. Incorporation of P1 lactam moieties as L-glutamine replacements. *J. Med. Chem.* **1999**, *42* (7), 1213−1224.

(15) Hoffman, R. L.; Kania, R. S.; Brothers, M. A.; Davies, J. F.; Ferre, R. A.; Gajiwala, K. S.; He, M.; Hogan, R. J.; Kozminski, K.; Li, L. Y.; et al. Discovery of Ketone-Based Covalent Inhibitors of Coronavirus 3CL Proteases for the Potential Therapeutic Treatment of COVID-19. *J. Med. Chem.* **2020**, *63* (21), 12725−12747.

(16) Chatterjee, A. K.; Chen, J. J.; Nakath, E.; Rahimi, A.; Gupta, A. K.; Grabovyi, G.; Wilson, K.; Ghorai, S.; Nazarian, A.; Pedoarena, J. et al. Protease inhibitors for treatment of coronavirus infections. US-11708348-B2, 2023.

(17) Yip, Y.; Victor, F.; Lamar, J.; Johnson, R.; Wang, Q. M.; Barket, D.; Glass, J.; Jin, L.; Liu, L.; Venable, D.; et al. Discovery of a novel bicycloproline P2 bearing peptidyl alpha-ketoamide LY514962 as HCV protease inhibitor. *Bioorg. Med. Chem. Lett.* **2004**, *14* (1), 251−256.

(18) McLaren, K. L. Total Synthesis of the Cyclic Depsipeptide Leualacin. *J. Org. Chem.* **1996**, *61* (8), 2914.

(19) Tuccinardi, T.; Granchi, C.; Rizzolio, F.; Caligiuri, I.; Battistello, V.; Toffoli, G.; Minutolo, F.; Macchia, M.; Martinelli, A. Identification and characterization of a new reversible MAGL inhibitor. *Bioorg. Med. Chem.* **2014**, *22* (13), 3285−3291.

(20) Owen, D. R.; Allerton, C. M. N.; Anderson, A. S.; Aschenbrenner, L.; Avery, M.; Berritt, S.; Boras, B.; Cardin, R. D.; Carlo, A.; Coffman, K. J.; et al. An oral SARS-CoV-2 M(pro) inhibitor clinical candidate for the treatment of COVID-19. *Science* **2021**, *374* (6575), 1586−1593.

https://doi.org/10.1021/acs.jmedchem.3c01938
J. Med. Chem. 2024, 67, 2369−2378